Advances in Nano Research, *Vol. 15, No. 5 (2023) 467-484*
https://doi.org/10.12989/anr.2023.15.5.467

Multiple effects of nano-silica on the pseudo-strain-hardening behavior of fiber-reinforced cementitious composites

Hossein Karimpour[a] and Moosa Mazloom*

Department of Structural and Earthquake Engineering, Faculty of Civil Engineering, Shahid Rajaee Teacher Training University, I. R. Iran

(*Received July 22, 2021, Revised June 22, 2023, Accepted August 14, 2023*)

Abstract. Despite the significant features of fiber-reinforced cementitious composites (FRCCs), including better mechanical, fractural, and durability performance, their high content of cement has restricted their use in the construction industry. Although ground granulated blast furnace slag (GGBFS) is considered the main supplementary cementitious material, its slow pozzolanic reaction stands against its application. The addition of nano-sized mineral modifiers, including nano-silica (NS), is an alternative to address the drawbacks of using GGBFS. The main object of this empirical and numerical research is to examine the effect of NS on the strain-hardening behavior of cementitious composites; ten mixes were designed, and five levels of NS were considered. This study proposes a new method, using a four-point bending test to assess the use of nano-silica (NS) on the flexural behavior, first cracking strength, fracture energy, and micromechanical parameters including interfacial friction bond strength and maximum bridging stress. Digital image correlation (DIC) was used for monitoring the initiation and propagation of the cracks. In addition, to attain a deep comprehension of fiber/matrix interaction, scanning electron microscope (SEM) analysis was used. It was discovered that using nano-silica (NS) in cementitious materials results in an enhancement in the matrix toughness, which prevents multiple cracking and, therefore, strain-hardening. In addition, adding NS enhanced the interfacial transition zone between matrix and fiber, leading to a higher interfacial friction bond strength, which helps multiple cracking in the composite due to the hydrophobic nature of polypropylene (PP) fibers. The findings of this research provide insight into finding the optimum percent of NS in which both ductility and high tensile strength of the composites would be satisfied. As a concluding remark, a new criterion is proposed, showing that the optimum value of nano-silica is 2%. The findings and proposed method of this study can facilitate the design and utilization of green cementitious composites in structures.

Keywords: cementitious composites; digital image correlation (DIC); fracture behavior; greenness; ground granulated blast furnace slag (GGBFS); micromechanics; nano-silica; strain hardening

1. Introduction

Fiber-reinforced cementitious composites (FRCCs) are cement-based composites with better mechanical properties than mortars and plain concretes due to the addition of short and discontinuous fibers. Even though fiber-reinforced concrete has a long history, a consistent expansion in the utilization of FRCC started in the 1960s. In comparison to unreinforced mortar or concrete, which fail in tension quickly after the initiation and propagation of a single crack, FRCCs have higher strength and ductility (Newman and Choo 2003).

Engineered cementitious composites (ECC) are a new category of FRCCs with strain-hardening properties that have appeared in recent years. This material is well-known for its ability to resist higher stresses, after the formation and propagation of cracks. However, most traditional fiber-reinforced concretes can withstand stresses after cracking, but at lower levels than first crack stresses (Fig. 1) (Li 2002).

This material utilizes short, randomly oriented fibers at a high amount (approximately 2 percent of total volume), and similar to steel, it has a resilient ductile performance under tension (Li 2002), which leads to an increase in structural safety potential in reinforced concrete (RC) structures subjected to earthquake (Li 2003a).

Despite all the merits mentioned, since coarse aggregates have been removed from ECC, these composites have a relatively large cement content. For reducing the use of cement, a systematic methodology for the development of green composite was proposed by Lepech *et al*. (2008). Three methods are suggested to reduce cement usage: (i) replacing part of the cement with supplementary cementitious materials (SCMs), (ii) replacing part of the cement with inert fillers, and (iii) cement replacement with alternate types of cement, producing lower carbon in proportion to consumed energy (Lepech *et al*. 2008; Li 2019). In ECC mixtures, the use of supplementary cementitious materials (SCMs) such as fly ash (FA), rice husk ash (RHA), and ground granulated blast-furnace slag (GGBFS) can partially replace cement.

GGBFS, a by-product of pig iron manufacturing, stands as a prominent choice among alternative materials for replacing cement. GGBFS has a pozzolanic reaction potential because it has an amorphous glassy-like micro-structure made of mono-silicates (Tsivilis *et al*. 2000).

*Corresponding author, Professor,
E-mail: Mazloom@sru.ac.ir
[a] Ph.D., E-mail: Karimpour.h@gmail.com

ISSN: 2287-237X (Print), 2287-2388 (Online)

When GGBFS mixes with PC, it increases the hydration rate and reacts with CH, one of the PC hydration products. Based on earlier studies, replacing PC with GGBFS up to 70% has no adverse effect on 28-day compressive strength. But the replacement of GGBFS reduces the strength of concrete at an early age (Swaddiwudhipong *et al*. 2003). Green ECC containing GGBFS and limestone powder has been studied by Zhou *et al*. (2010). It was found that with increasing the replacement of GGBFS instead of cement (range between 50 to 70%), the tensile strain capacity generally increases. With the use of micromechanics principles, a composite with a strain capacity of 3.3% with a crack width of 57 μm was designed (Zhou *et al*. 2010). Kim *et al*. (2007) conducted research in which ground granulated blast furnace slag (GGBFS) substituted FA in ECC. They optimized the range of GGBFS-ECC mixture proportion based on micromechanics. It was shown that both the ductility and tensile strength of the GGBFS-ECC are significantly higher than these values for the ECC without GGBFS. Moreover, the GGBFS-ECC shows a lower matrix fracture toughness (J_{tip}). Therefore, GGBFS-ECC demonstrated a higher toughness ratio in comparison with ECC without GGBFS. It could be concluded that the use of GGBFS particles could be beneficial for strain-hardening behavior. This implies that as the toughness increases, the probability of experiencing multiple cracks in the composite also increases. Furthermore, it was acknowledged that the utilization of GGBFS exerts a beneficial influence on fiber dispersion, creating a driving force that enhances overall workability. This is due to an electrical double layer made by the oxidized slag surface.

In contrast to Portland cement, the pozzolanic reaction of FA and GBBFS is a slow process that contributes to strength only at later ages. Furthermore, if large amounts of pozzolanic materials are used, the early-age strength of ECC decreases, limiting the widespread use of green cementitious composites by engineers (Poon *et al*. 2000, Yang *et al*. 2007). As a result, the mixture design of ECC specimens must be carefully optimized to minimize these drawbacks (Zhang *et al*. 2000, Hanehara *et al*. 2001).

The addition of nano-sized mineral modifiers has been extensively researched as a potential solution for enhancing the performance of cementitious composites, particularly at early ages (Hejazi *et al*. 2012, Kawashima *et al*. 2013). The impact of nano-silica on the initial stages of cement hydration was investigated by Torabian Esfahani *et al*. (2017). The findings of this research revealed that cement pastes containing 1.5 percent nano-silica experienced a 37.5 percent increase in compression strength after just 3 days, compared to pastes without nano-silica. Interestingly, while the 28-day compressive strength also increased by 14.6 percent in the cement paste with 1.5 percent nano-silica compared to the control paste, the early-stage effect was much more pronounced.

It has been discovered that using nano-silica (NS) in cementitious materials can result in denser packing of hydration products, pore refinement, and an enhanced interfacial transition zone (ITZ). The ITZ occurs between the hardened paste and the fibers in FRCCs (Ji 2005, Jo *et al*. 2007, Flores-Vivian *et al*. 2013, Abna and Mazloom 2022). The available CH ($Ca(OH)_2$) produced during cement hydration is consumed by NS, resulting in a hydrated calcium silicate (C-S-H) gel. calcium hydroxide (CH) consumption speeds up cement hydration, because CH is the hydration product of cement. Thus, greater amounts of C-S-H gels could be formed In composites. In another way, NS particles provide a seeding surface due to their very tiny particle size, accelerating hydration with accelerated pozzolanic activity (Goh and You 2009). The created C-S-H gels gradually fill the detrimental pores in the matrix leading to an enhancement in the durability of the cementitious matrix (Mohammed *et al*. 2017).

NS is also often prescribed as a viscosity-modifying admixture (Ji 2005). Because of the higher surface area of the NS, adding nanoparticles leads to good workability in high-strength and high-flowable concrete without segregation. When flowable concrete is required, this can be advantageous since greater amounts of super-plasticizer (SP) can be used in such mixtures without segregation (Ji 2005).

Based on the Mercury intrusion porosimetry (MIP) results, Li *et al*. (2016) discovered that when NS particles are added to the composite paste, the changing trend of porosity is opposite to pore size. In fact, porosity variation is largely attributed to gel pores. NS helps to reduce the pore sizes and improves the microstructure, but C-S-H has a lot of gel pores, Thus, increasing C-S-H gel leads to an increase in the porosity. Nevertheless, due to their remarkably small sizes, these gel pores have no negative impact on the microstructure and mechanical properties of cement-based materials (Li *et al*. 2016).

In FRCC, the presence of fibers can create a more complex microstructure, with the potential for fiber-matrix debonding and fiber pullout. Nano-silica can help to improve the interfacial bonding between the fibers and matrix and enhance the overall mechanical properties of the composite. The higher percentages of nano-silica used in FRCC rather than normal concrete can be attributed to this need for improved interfacial bonding, and the desire to achieve optimal mechanical performance (Chaoshu *et al*. 2021). Cementitious composites with strain-hardening behavior have been made based on micromechanical models. According to the principles governing the mechanics-based principles, the maximum tensile cracking strength must not exceed the maximum fiber bridging strength (Wang and Li 2007). This implies that the cementitious matrix's strength must be limited to satisfy the models. Fracture localization occurs when the tensile load required to initiate a new crack exceeds the capacity of bridging fibers at any of the multiple cracks that have already formed (Li 2019).

The main objective of this research is to tackle the limitations and challenges that hinder the widespread use of cementitious composites. These challenges include the high cost of fibers (i.e., polyvinyl alcohol (PVA) fibers) used in the composition of cementitious composites and their low strength at early stages. To overcome these issues, this study proposes the use of a strain-hardening composite reinforced with polypropylene fibers and a green binder/filler. The aim is to enhance the environmental sustainability of strain-

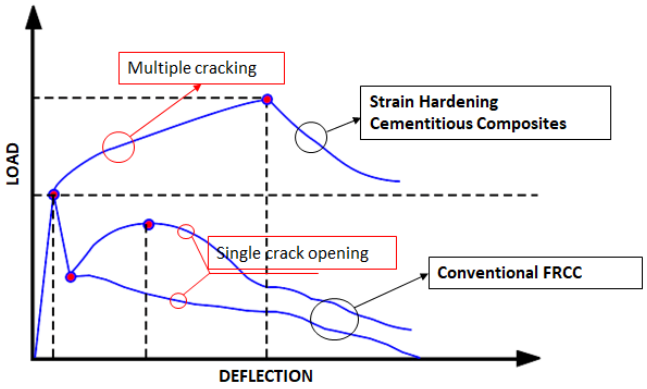

Fig. 1 typical load-displacement curves of FRCCs

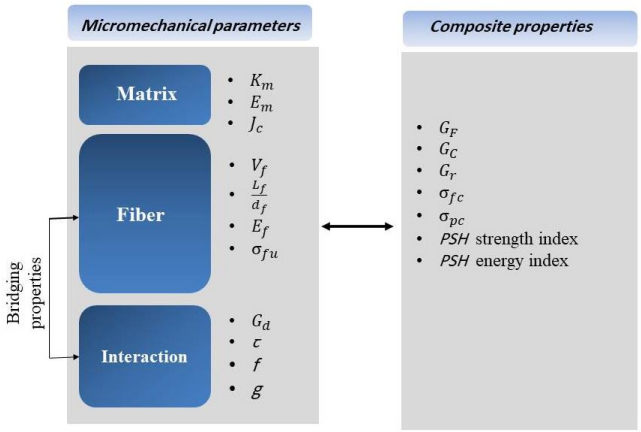

Fig. 2 the design approach of cementitious composites based on micromechanics

hardening composites and to make them more cost-effective, thereby increasing their potential for practical application. The matrix was modified to decrease the adverse effects of GGBFS and enhance the properties of cementitious composites. The addition of NS, despite all its advantages, leads to an increase in fracture toughness, compression, and tension strength of the cement-based matrix. According to previous research based on micro-mechanics, strengthening the cementitious matrix prevents the emergence of multiple cracking and, therefore, strain-hardening. In this manner, the research presented in this paper concentrated on the effects of different NS weight fractions on various ECC properties and relative better-ments in the presence of GGBFS. Modified ECC mixtures with different NS weight fractions were created to optimize the composite's strain-hardening behavior. Moreover, this paper supposes a novel technique to investigate the micro-mechanical parameters from fractural tests. To achieve this goal, mechanical and fracture properties testing was conducted, and the resulting data were analyzed using both fractural and micromechanical concepts. A new criterion is supposed to find the optimum NS content for enhancing both the ductility and tensile strength of cementitious composites. Digital image correlation (DIC) was utilized to capture the crack pattern and the first crack load for finding the first crack stress.

DIC, an optical-numerical displacement measurement technique, has become increasingly prevalent in the field of experimental mechanics. Past research has demonstrated the remarkable precision of the DIC technique in characterizing cement-based specimens in both hardened and fresh states (Chiranjeevi Reddy and Subramaniam 2017, Mitrović *et al.* 2019, Bhosale *et al.* 2020, Qing *et al.* 2021, Karimpour and Mazloom 2022a). This method eliminates the need for complex and expensive equipment, making it an attractive option for high-precision measurements.

2. The analytical formulations for finding the impact of NS on the micromechanical properties of cementitious composites

2.1 Micromechanics-based analysis methodology

The ductile composites' design is based on the synergy of mechanical interactions between the matrix, fiber, and composite interfaces to attain multiple cracking in tension. The micromechanical design provides an imperative link between material structures and composite properties (Fig. 2). It allows the design of ductile composites for diverse performance without relying on trial and error, pervading fiber-reinforced concrete studies, which is costly and time-consuming (Li 2019). For optimizing the composite's behavior, the micromechanical relations are extracted from the literature, revised, and adapted to the composites' ingredients.

The main effect of fibers is that they act as bridging elements (ligaments) behind the crack tip and prevent the growth of cracks and resist their propagation. Consequently, fiber-reinforced composites' structural performance is strictly controlled by the bridging behavior of the fibers that cross the matrix crack. The composite bridging stresses originate from the composite fibers crossing the crack, which has a certain amount corresponding to the specific amount of crack opening (Zhang and Li 2002).

Li (1992) investigated the relationship between fiber bridging load and displacement through fiber frictional debonding and fiber pull-out. The following assumptions are used to build the micromechanics model: (i) Fibers never break, (ii) During the debonding and pull-out processes, the interfacial friction bond strength along the fiber-matrix interface remains constant. For a composite with fiber volume fraction V_f, Li *et al.* (1991) demonstrated that the relation between bridging stress σ_B and displacement δ can be derived by integrating over the contributions of only those individual fibers that cross the crack plane of the matrix:

$$\sigma_B(\delta) = \frac{4V_f}{\pi d_f^2} \int_{\varphi=0}^{\pi/2} \int_{z=0}^{\left(\frac{L_f}{2}\right)\cos\varphi} p(\delta)\, p(\varphi) p(z) dz d\varphi \qquad (1)$$

where d_f and L_f are fiber diameter and fiber length, respectively. Fig. 3 shows an inclined fiber, demonstrating inclination angle φ and centroidal distance z. $p(\varphi)$ and $p(z)$ correspond to probability density functions of the orientation angle and centroidal distance of fibers from the crack plane. For uniform random distributions, $p(\varphi) =$

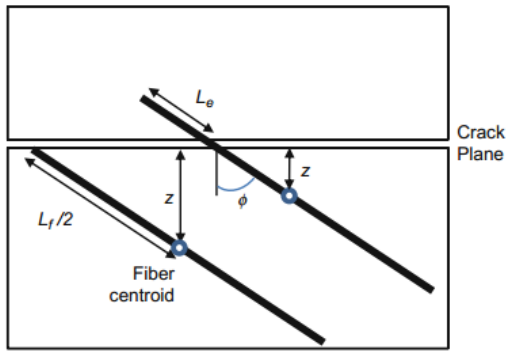

Fig. 3 A fiber crossing a matrix crack and its centroid position (Li 2019)

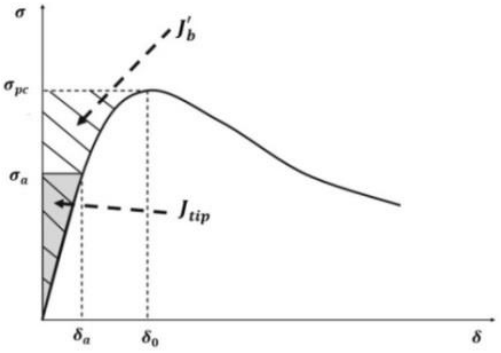

Fig. 4 Typical $\sigma(\delta)$ curve for tensile strain-hardening composite

$\sin\varphi$, and $p(z) = \frac{L_f}{2}$ (Li *et al*. 1991). The pre-peak and post-peak part of the bridging stress–displacement curve $(\sigma_B - \delta)$ can then be obtained in a normalized form as follows (Li 1992).

$$\overline{\sigma}_B(\overline{\delta}) = g\left[2\left(\frac{\overline{\delta}}{\overline{\delta}^*}\right)^{\frac{1}{2}} - \frac{\overline{\delta}}{\overline{\delta}^*}\right] \quad \text{For} \quad \overline{\delta} \le \overline{\delta}^* \tag{2}$$

$$\overline{\sigma}_B(\overline{\delta}) = g(1-\overline{\delta})^2 \quad \text{For } 1>\overline{\delta}>\overline{\delta}^* \tag{3}$$

where normal bridging stress $\overline{\sigma}_B = \sigma_B/\sigma_0$, $\sigma_0 = V_f\tau(L_f/d_f)/2$, and $\overline{\delta} = \delta/(L_f/2)$. d_f and L_f are fiber diameter and fiber length, respectively. $\overline{\delta}^* = \tau[(1+\eta)/E_f]\left(\frac{L_f}{d_f}\right)$ corresponds to the maximum attainable value of σ_0 normalized by $L_f/2$. The elastic modulus of the matrix and the fiber are E_m and E_f, respectively, and the volume fraction of the matrix and the fiber are V_m and V_f, respectively and $\eta = (V_fE_f/V_mE_m)$. τ is the interfacial friction bond strength. The maximum value of bridging stress σ_{pc}, is often referred to as the composite post crack strength and is obtained by:

$$\sigma_{pc} = \frac{1}{2}g\tau V_f\left(\frac{L_f}{d_f}\right) \tag{4}$$

In Eqs. (2)-(4), the snubbing factor g can be inferred physically as the increase in bridging force across a matrix crack when a fiber is pulled out at an inclined angle, similar to a flexible rope passing over a friction pulley. The snubbing coefficient f, obtained experimentally, is used to determine the snubbing factor g (Li 1992).

$$g = \frac{2}{4+f^2}(1+e^{\pi f/2}) \tag{5}$$

Marshall and Cox (1988) have shown that the stress required to extend the first matrix crack (i.e., the onset of damage is a decreasing function of the crack size if the crack is small, but approaches a constant "steady-state" value for large cracks. Marshall and Cox (1988) presented a simple derivation of a general solution for the steady-state matrix cracking stress. The solution was obtained by the use of the J-integral (Rice 1968). Based on the J-integral method, the crack tip toughness J_{tip} during steady-state cracking can be expressed by:

$$J_{tip} = \sigma_a\delta_a - \int_0^{\delta_a}\sigma_B(\delta)\,d\delta \tag{6}$$

where σ_a is the steady-state cracking stress, and δ_a is the displacement corresponding to σ_a (Fig. 3) (Pan *et al*. 2015). Li (1993) discussed the conditions required for pseudo-strain-hardening behavior. These two conditions must be met for pseudo-strain-hardening with multiple cracking to occur.

$$\sigma_a \le \sigma_{pc} \tag{7}$$

$$J_{tip} \le \sigma_{pc}\delta^* - \int_0^{\delta^*}\sigma_B(\delta)\,d\delta = J_b' \tag{8}$$

where $J_{tip} = \frac{k_m^2}{E_m}$ and k_m is the matrix fracture toughness, and E_m is the matrix Young's modulus. The first requirement is that the composite must exhibit crack bridging that exceeds the first cracking stress to prevent immediate failure upon the initiation of a microcrack from an initial flaw in the matrix. The second criterion is that the composite must have sufficient energy to generate the steady-state crack condition that is necessary for multiple cracking to occur. This concept is illustrated in Fig. 4, which depicts the $(\sigma_B - \delta)$ curve.

The complementary energy (J_b') can be calculated as follows:

$$J_b' = V_f\left(\frac{l_f}{d_f}\right)\left(\frac{\tau^2 l_f^2}{6E_f d_f} - 2G_d\right) \tag{9}$$

Due to the random nature of pre-existing flaw size and fiber distribution in cement composites, a large margin between J_b' and J_{tip} as well σ_{fc} and σ_{pc} is preferred. The pseudo-strain-hardening (PSH) performance index was used to quantify the margin and is defined as follows (Yang and Li 2010):

$$\text{PSH energy} = \frac{J_b'}{J_{tip}} \tag{10}$$

$$\text{PSH strength} = \frac{\sigma_{pc}}{\sigma_{fc}} \tag{11}$$

where σ_{fc} is matrix first cracking strength and J_b' is the complementary energy calculated from the bridging stresses

σ versus crack opening δ curve. Materials with higher PSH indices should be more prone to saturated multiple cracking. Unsaturated PSH behavior frequently results in low tensile strain capacity and high variability in tensile ductility of composites (Yang and Li 2010).

2.2 Fracture energy

The fracture energy of materials is the energy required to create a unit area of the crack and determines crack propagation's energy consumption (Karamloo and Mazloom 2018, Salehi and Mazloom 2018). It can play a vital role in the fracture behavior of the material. In recent years, scholars have studied the fracture behavior of various types of quasi-brittle materials such as concrete, self-compacting normal, and lightweight concrete (Mazloom *et al*. 2018, Naniz and Mazloom 2018, Mazloom and Salehi 2018).

2.2.1 Finding the total fracture energy using work of fracture method

The work of fracture method is the most common experiment to define the fracture properties of concrete, which is proposed as a standard (RILEM 1985). The basis for applying this method to concrete was developed by Hillerborg (1985). Their approach uses the "fictitious crack" concept (Hillerborg *et al*. 1976, Hillerborg 1980, Petersson 1981). The use of work of fracture method is not limited only to plain concrete.

Mazloom *et al*. (2020) used the work of fracture method to investigate the fracture behavior of monotype and hybrid fiber reinforced self-compacting concrete at various temperatures. Experimental results showed that fracture energy has a strong correlation with fiber volume content and temperature (Mazloom and Mirzamohammadi 2019, 2021). The fracture energy of fiber-reinforced cementitious composites with varying fiber lengths and volumes was studied by Karimpour and Mazloom (2022a) to improve the strain-hardening behavior, and the results were analyzed using the work of fracture method and micromechanics. The fracture energy should be considered as:

$$G_F = \frac{W_F}{A_{lig}} = \frac{W_0 + mg\delta_0}{(H - a_0)B} \quad (12)$$

in which W_F = the overall work performed by all the loads involved, W_0 = area under lload-displacement curve up to δ_0, mg = the sum of the loads that perform secondary work, including beam and instrument weight, δ_0 = the displacement at failure, A_{lig} = the ligament area, H = the height, a_0 = the initial crack length, and B = the width of the specimen (Karimpour and Mazloom 2022b).

2.2.2 Finding the debonding and pull-put fracture energy using micromechanics

The fracture energy due to fiber pull-out can be computed from Eq. 13:

$$G_C = \int_0^{l_f/2} \sigma_B(\delta)\, d\delta \quad (13)$$

And with $\sigma_B(\delta)$ given by Eq. 3, it can be shown that:

$$G_C = \frac{1}{12} g\tau V_f d_f \left(\frac{L_f}{d_f}\right)^2 \quad (14)$$

Part of the fracture energy spent on the fiber bonding process may be estimated by integrating the pre-peak stress-displacement curve (Eq. 2) for δ up to δ^*. The result is:

$$G_r = \frac{5}{12} g\tau V_f d_f \left(\frac{L_f}{d_f}\right)^2 \bar{\delta}^* \quad (15)$$

Comparison with (Eq. 14) indicates that this part of the fracture energy is negligibly small, of the order of δ^*.

2.2.3 Finding the pull-out fracture energy G_C from the load-displacement curve

As shown in Fig. 5, strain-hardening composites exhibit linear load displacement or stress-strain during loading the notched beam until the matrix starts to crack. Then non-linear load-displacement or stress strain continues as the matrix demonstrates multiple micro-cracks, with the attendant decrease in the composite modulus. The critical point on the composite stress-strain curve is the point of the first micro-cracking of the matrix. This is sometimes referred to as the "micro-crack yield stress" or "proportional limit." At this point, some fiber-matrix debonding occurs, and the fibers bridge the advancing tensile cracks in the matrix, exerting closure forces to restrict crack opening. Fiber pull-out occurs during the subsequent propagation of matrix cracks.

As can be seen from Fig. 5, according to laboratory observations, the unreinforced matrix has a brittle behavior. However, in the fiber-reinforced notched beam under monotonic loading, by reaching the maximum load, the formed cracks open, and the process of fiber pull-out happens. Therefore, in this study, it is suggested that the area under the load-displacement curve after the maximum load would be considered as the pull-out work. As a result, the pull-out fracture energy is calculated from the following equation:

$$G_C = \frac{W_C}{A_{lig}} \quad (16)$$

2.3 Finding the fracture toughness of the matrix

For finding the fracture toughness of the matrix, the following equations are suggested in the previous works (Rooke and Cartwright 1976, Yon *et al*. 1997):

$$K_c = f\left(\frac{a}{w}\right)\frac{3ps\sqrt{a}}{2tw^2} \quad (17)$$

where K_c is the stress intensity factor, (P) the failure load, S the length of the span, (a) the length of the crack, w the specimen width, t the thickness, and $f\left(\frac{a}{w}\right)$ is a geometric factor for each kind of specimen that can be calculated through this equation for the notched beam under four-point loading (Rooke and Cartwright 1976):

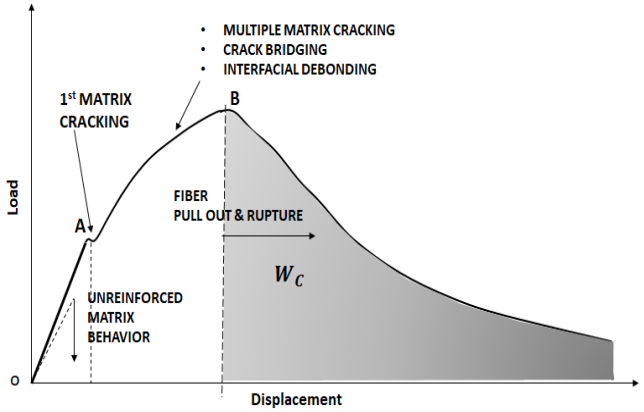

Fig. 5 Load–displacement curve of strain-hardening cementitious composites during loading, the related failure, and the defined pull-out work in the present study (schematic)

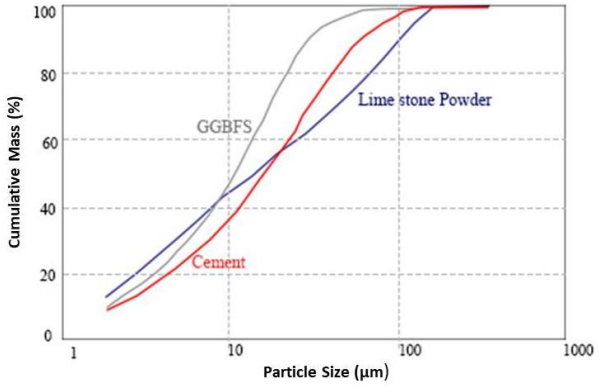

Fig. 6 Particle size distribution of the powder materials in the cementitious composites

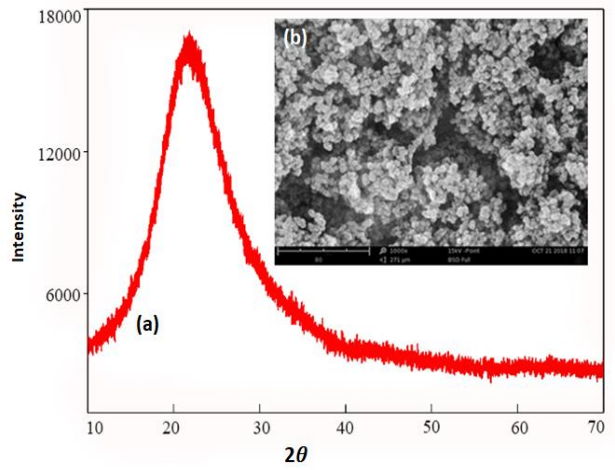

Fig. 7 (a) XRD diagram of the crystal structure of NS, (b) SEM photograph of NS

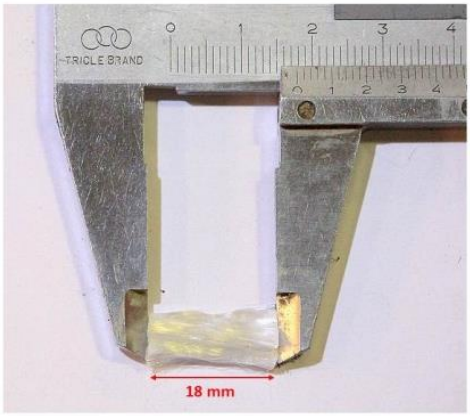

Fig. 8 PP fibers with 18 mm length

$$f\left(\frac{a}{w}\right) = 1.12 - 1.39\left(\frac{a}{w}\right) + 7.32\left(\frac{a}{w}\right)^2 - 13.1\left(\frac{a}{w}\right)^3 + 14\left(\frac{a}{w}\right)^4 \quad (18)$$

3. Experimental program

3.1 The raw materials

Portland cement-I (PC-I), limestone powder (LP), ground granulated blast furnace slag (GGBFS), high range water reducer admixture (HRWRA), and polypropylene (PP) fibers were used as constituents of the cement-based matrix in the composite production. Limestone powder is made by finely grinding limestone and is mainly composed of calcium carbonate ($CaCO_3$). The limestone powder is often referred to as an inert filler material because it undergoes minimal reaction with cement clinker or hydration products (Poppe and De Schutter 2005). Carboxylate-based High Range Water Reducer (HRWR), with the commercial name of SRT-2912, was used as the super-plasticizer. Chemical Analysis and physical properties of solid materials are given in Tables 1 and 2. Fig. 6 depicts the particle size distributions of GGBFS, LP, and PC. As can be seen, the sizes of the fine particles gradually increased, and the fiber-matrix interface is strengthened as a result of the increased particle packing density. This study is carried out based on the ECC mix proportion, in which the amount of Portland cement is lower than 15% of powder materials by weight. NS in powder form with an average particle size of approximately 20 ± 5 nm was incorporated into ECC mixtures to illustrate their effect on the mechanical and micromechanical properties of cementitious composites. Chemical analysis of NS is depicted in Table 1. NS X-ray diffraction (XRD) results and scanning electronic micrograph (SEM) of NS are depicted in Fig. 7. As is apparent from Fig. 7, NS particles did not exhibit pronounced crystalline peaks suggesting that these particles are mainly amorphous in nature.

The objective of this study is to achieve strain hardening behavior in green cementitious composites by incorporating PP fibers (Fig. 8). Table 3 provides detailed information on the properties of PP fibers. According to the data presented in Table 3, the hydrophobic nature of PP fibers results in a reduced tendency to absorb water and adhere to hydrophilic cementitious materials (Pakravan and Ozbakkaloglu 2019). PP fibers were 18 mm long and 35 μm in diameter, resulting in a L_f/d_f of 514, which was significantly higher than the commonly used PVA fiber's L_f/d_f of around 300 (Li 2003b).

Table 1 Chemical analysis of cement, GGBFS, and NS

Component (%)	Sio_2	Al_2o_3	Fe_2O_3	Cao	MgO	Na_2O	K_2O	SO_3	L.O.I*
Cement	21.32	3.83	2.96	62.02	3.44	0.42	0.71	2.09	2.4
GGBFS	35.05	10.36	0.85	35-37	10.25	0.5	0.35	1.85	2.1
LP	0.07	0.00	0.02	56.9	0.13	0.07	0.00	0.05	42.73
nano-SiO_2	99.17	0.38	0.02	0.00	0.21	0.09	0.00	0.00	-

*loss Of Ignition

Table 2 GGBFS and cement physical characteristics

	Specific gravity	Fineness(cm^2/gr)	Amorphous phase
GGBFS	2.58	3800	90%
Cement	3.15	3307	-

Table 3 PP fiber properties

Specific gravity	0.91	Tensile strength (MPa)	350-400
Length(mm)	18	Module of elasticity (GPa)	3-3.5
Diameter(mm)	0.035	Elongation (%)	20
color	white	Acid and alkaline resistance	Excellent
Melt point (c^o)	160-170	Water absorption	No

Table 4 Mix proportion of a PP-ECC made with PC-GGBFS-LP and different amounts of NS (material weight (kg) per $1m^3$ of composite)

Mix Id	cement	Limestone powder	GGBFS	Water/powder Ratio	Super-plasticizer	PP fiber	NS	NS (%)
NS-0, V-2	342.6	1142	799.4	0.26	11.42	18.2	0.0	0
NS-1,V-2	342.6	1142	799.4	0.26	11.42	18.2	3.4	1
NS-2,V-2	342.6	1142	799.4	0.26	11.42	18.2	6.9	2
NS-3, V-2	342.6	1142	799.4	0.26	11.42	18.2	10.3	3
NS-4, V-2	342.6	1142	799.4	0.26	11.42	18.2	13.7	4
NS-0, V-0	342.6	1142	799.4	0.26	5.71	18.2	0.0	0
NS-1, V-0	342.6	1142	799.4	0.26	5.71	18.2	3.4	1
NS-2, V-0	342.6	1142	799.4	0.26	5.71	18.2	6.9	2
NS-3, V-0	342.6	1142	799.4	0.26	5.71	18.2	10.3	3
NS-4, V-0	342.6	1142	799.4	0.26	5.71	18.2	13.7	4

At the same fiber volume fraction, a higher L_f /d_f ratio produced a greater fiber-matrix interfacial area, increasing fiber-bridging capacity (Naaman and Najm 1991, Lin and Li 1997).

3.2 Mixture proportion and mixing procedure

As a result of this research, an ECC mix proportion with a Portland cement content as low as 15% of powder by weight has been produced. Table 4 shows the compositions of the mixtures. In the mixes shown in Table 4, NS was added to the mixture based on cement percent. In naming mixes, the letter NS indicates the percent of NS, adding to the mixture by the weight of cement, and the letter V indicates the volume content of the fibers.

Mixing sequence has a significant effect on cement composites. As a result, the adjustment to the mixing sequence is an alternate solution to achieve a higher viscosity for improvement in fiber dispersion. Zhou *et al*. (2012) suggested holding back some water to raise the plastic viscosity to an appropriate level when fiber was added. The remaining water was added only after the fibers had been thoroughly mixed. Changing the mixing sequence might seem simple, but it affected the tensile strain capacity of ECC dramatically. Fiber distribution analyses at the cross-section of the specimens indicated a significant correlation between improvement in the dispersion of the fibers and growth in tensile strain capacity using the adjusted mixing process (Zhou *et al*. 2010).

The dispersion of nanomaterial is an essential aspect of the manufacturing process of nano-modified composites. Discrepancies in findings from one study group to another can be due to the distribution methods. Agglomeration is common in nanomaterial due to their high Van der Waals

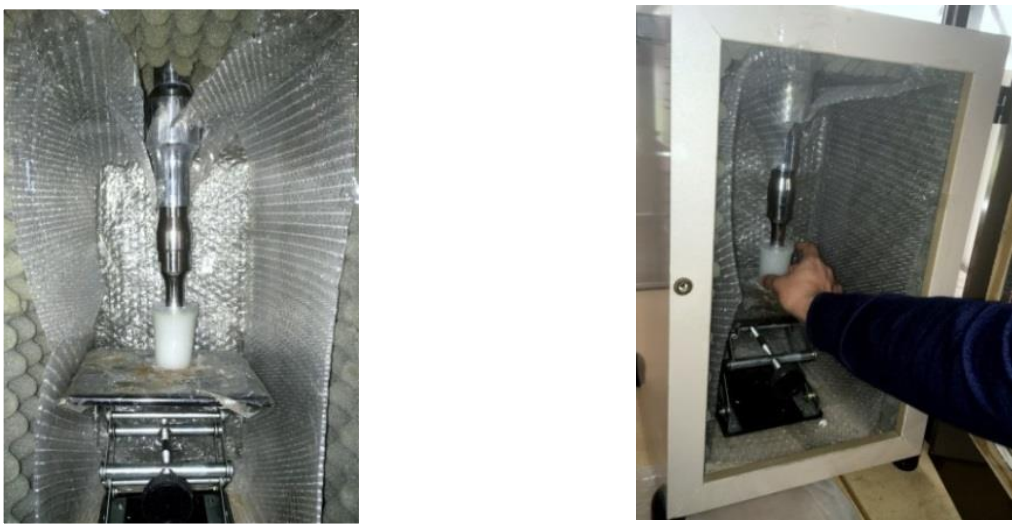

Fig. 9 Sonication of water and NS by an ultrasonic homogenizer

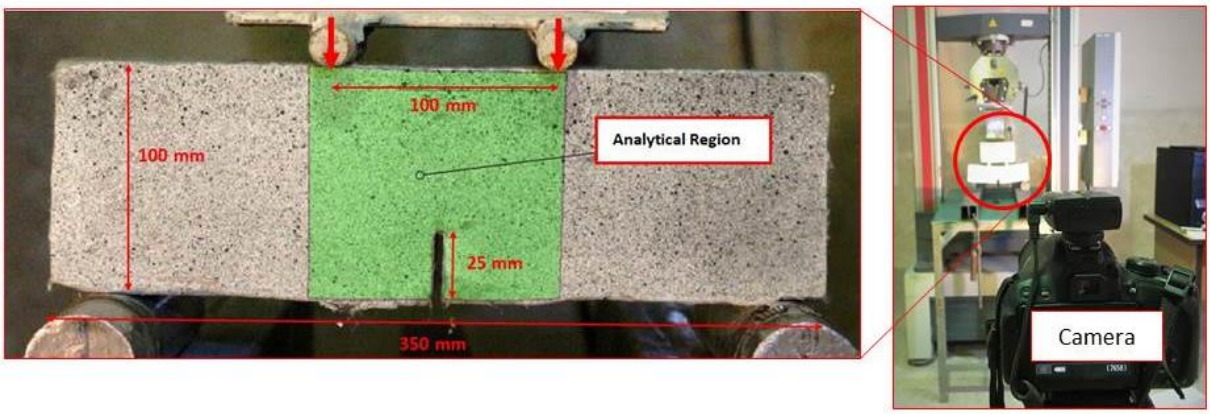

Fig. 10 Experimental set up for displacement-control four-point bending test

forces. The efficiency of nanomaterial is reduced by agglomeration. Ultra-sonication and the use of surfactants are frequently used to achieve effective dispersion. To disperse particles, sonification relies on mechanical vibrations that generate high levels of energy (high-frequency vibrations). Surfactants prevent particles from re-agglomerating by increasing chemical repulsion between them. Nonetheless, the surfactant could become attached to these nanoparticles, leading to the creation of consumed surfactants that are ineffective during the mixing process. Furthermore, ultra-sonication of the surfactant may affect a change in chemical and physical properties affecting its performance in a cement-based mixture (Shah *et al*. 2009). Due to this, the mixing sequences of materials were as follows:

a. All amounts of water, indicated in Table 4 were ultra-sonicated with NS, (Fig. 9 demonstrate the ultra-sonic homogenizer used in this research)

b. By using a separate mortar mixer, half the amount of powder materials was mixed.

c. Half amount of water ultra-sonicated with NS added and mixed to obtain the desired viscosity for proper fiber distribution.

d. In the following step, the fibers were added to the mixture.

e. After the fibers were mixed homogeneously, the rest of the powder and liquid materials were added, contrary to the usual procedure where the fibers are added in the last step.

3.3 Test procedure

The 28-day compressive strengths of the green cementitious composite were determined using three cylindrical specimens with a diameter of 100 mm and a height of 200 mm for each mix. Four-point bending tests were carried out on prism specimens including 27 fiber-reinforced composite and three matrix-only specimens with dimensions of 350*100*100 mm and a free span of 300 mm. The samples' notches were made in the middle of their lengths using an acrylic plate with a thickness of 3 mm and a height of 25 mm during casting. All of the specimens were cured underwater for 28 days at $20 \pm 2^{o}C$.

All 4-point bending samples were tested under displacement-controlled conditions by a servo-controlled universal testing machine. The speed of the test was 0.1 mm/min to obtain the post-peak part of the load-displacement curve completely. The test setup of this research is shown in Fig. 10. According to ASTM C1609,

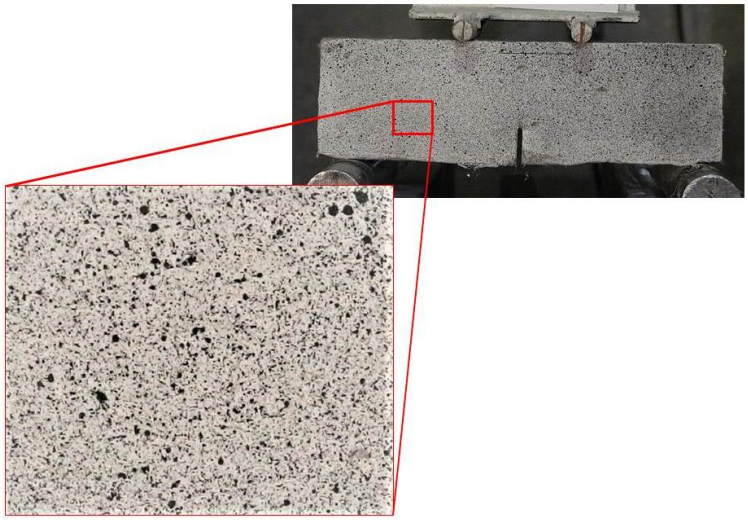

Fig. 11 An evenly distributed speckle pattern on the surface of the beam

the deflection equal to $\frac{l}{150}$ is the end of test for normal concrete with fiber, this point is equal to 2 mm in this study, but due to the high capacity of fiber reinforced cementitious composite in comparison with normal concrete, tests ended when the crack length reached 80 percent of the beam's depth. The equipment's weight considered in the calculation of fracture energy was 10 kg, which was negligible compared to the applied loads.

Digital Image Correlation (DIC) was utilized to calculate the displacement field and monitor crack propagation. The approach is based on a comparison of images taken when an object is being loaded. The object of interest must be covered with painted speckles to make the method works properly. As a result, an evenly distributed speckle pattern was randomly sprayed on the specimens' flat white surface (Fig. 11). Multiple photographs of crack formation and growth were captured using a DSLR camera positioned perpendicular to the specimen during the test, at a rate of one shot per second. Through the analysis of these images, the first crack load and cracking pattern were determined. The DIC calibration was completed by using certified distances on the specimen, and the output data were validated by comparing them to data obtained from the universal test machine.

4. Results and discussion

4.1 Fresh properties

The fresh properties of nano-modified cementitious composites are shown in table 5. The perpendicular diameters of the resulting flow are d_1 and d_2 as depicted in Fig. 12. In this research for evaluating the effect of NS content on the fresh and hardened properties of cementitious composites, values of W/B and SP amount are fixed in all of the mixtures of cementitious composites. The measured slump spread for mixtures is within the range of 685 mm to 750 mm, which is consistent with self-compacting specifications. The results showed that the inclusion of NS particles improved the cohesiveness of the mixtures in the fresh state, while decreased the slump spread. Pourjavadi *et al*. (2012) reported a similar trend for composites modified with 0.5-1 percent NS particles. This behavior confirms the fact that the amount of lubricating water available in the mixture is reduced when NS is added (Senff *et al*. 2009).

NS particles have a high surface area, adding them to cement mixtures necessitates the addition of more water or chemical admixtures to maintain the mixture's workability (Neville 1996, Mehta and Monteiro 2017). If the water content remains constant, as in the actual conditions, increasing the NS content promotes particle packing, reducing the volume between them and lowering the free water. As a result, there is more internal friction between solid particles (Qing *et al*. 2007, Senff *et al*. 2009, Diamantonis *et al*. 2010).

4.2 Compression strength

The 28-day compressive strengths of mixes are shown in Fig. 13. According to Fig. 13, the addition of NS increased the compressive strength of cementitious composites. The optimal value of NS content was at 3%. When the content of NS increased more (i.e., 4%), the compressive strength decreased by 5.1% in comparison with that of the (NS-3) sample. The filling effect, as well as the chemical effect associated with NS, could be responsible for the increased strength. In fact, as a Nano-filler, nano-particles of SiO_2 can fill the spaces between particles of C-S-H gel. Moreover, the amount of C–S–H increases as a result of the pozzolanic reaction with calcium hydroxide, resulting in higher matrix densification, which enhances the material's strength and durability (Neville 1996, Björnström *et al*. 2004, Li 2004).

The difficulty in uniform dispersion may account for the less positive effect of NS's higher dosage (i.e., 4%) on the compressive strength of the composites. However, as is sho wn in Fig. 14 in the mortars, the composites' paste, the com pressive strength had a rising trend with the increase of NS content. A possible explanation for this might be that the

Table 5 The measured slump spread for the mixes with different NS content

Mix Id	Slump spread		
	d_1 (mm)	d_2 (mm)	S (mm)
NS-0, V-2	752	748	750
NS-1, V-2	736	734	735
NS-2, V-2	724	720	722
NS-3, V-2	713	709	711
NS-4, V-2	687	683	685

$S = \frac{s_1+s_2}{2}$ Where s is the slump spread

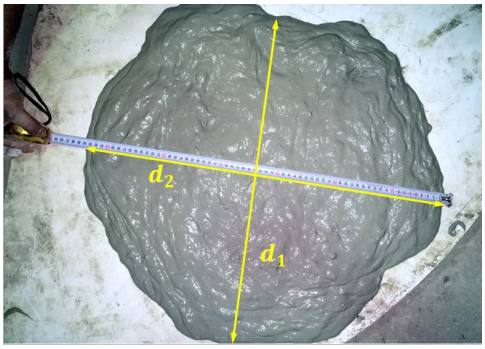

Fig. 12 Slump flow test of fresh composite

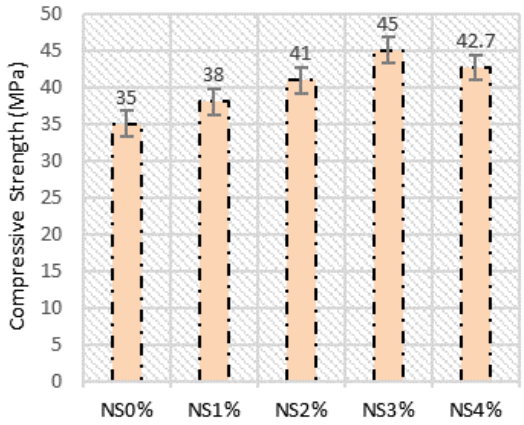

Fig. 13 Compressive strength of cementitious composites containing different amounts of NS

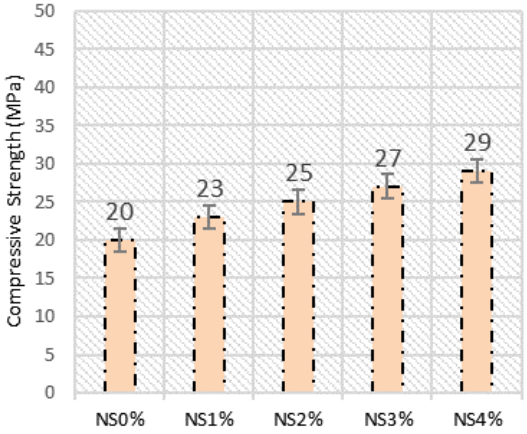

Fig. 14 Compressive strength of mortars containing different amounts of NS

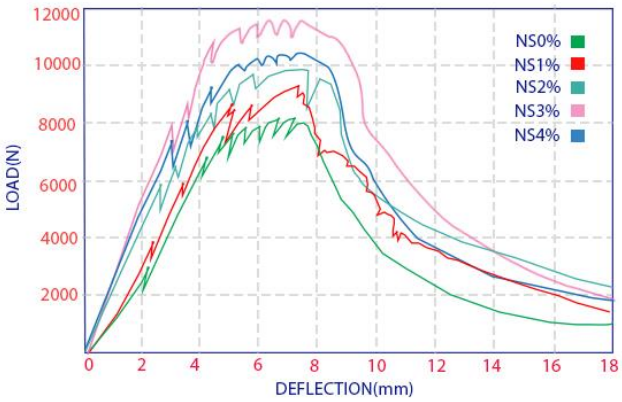

Fig. 15 Experimental load-displacement curves for composites with different percentages of NS

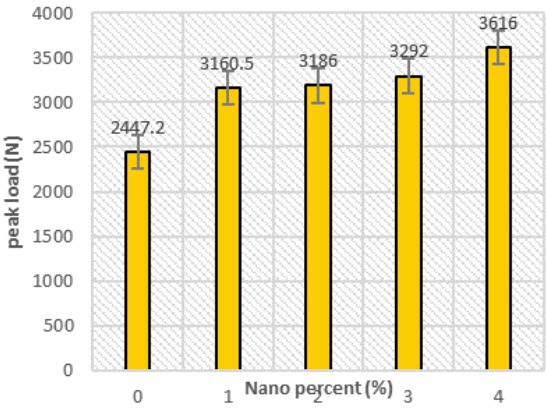

Fig. 16 Peak loads of matrix-only specimens with different percentages of NS

dispersion of NS particles is much better than that of fiber-reinforced cementitious composites.

4.3 Flexural behavior of the notched beams

Ten mixes were designed with the variables of NS percent. Thirty notched beams, including 15 fiber-reinforced composite specimens and 15 matrix-only specimens were cast and tested. The average load-displacement curves of fiber-reinforced notched beams with different NS percent are given in Fig. 15. The peak loads in matrix-only and fiber-reinforced specimens are demonstrated in Fig. 16 and Fig. 17, respectively. As is obvious, with the increasing percentage of NS, the peak loads of matrix-only specimens increased. However, the maximum load in fiber-reinforced cementitious composite increased with increasing NS up to 3% and then showed a downward trend. Table 6 demonstrates the flexural strength of the Nano-modified and unmodified samples. The flexural strength of fiber-reinforced composites has an optimum point that existed in 3%. Fig. 18 provides the comparison between flexural strength of the matrix and cementitious composite with increasing NS. It has been shown through the results that the flexural strength of cementitious composites can be improved by incorporating nano silica up to a certain optimal percentage, which improves the microstructure and

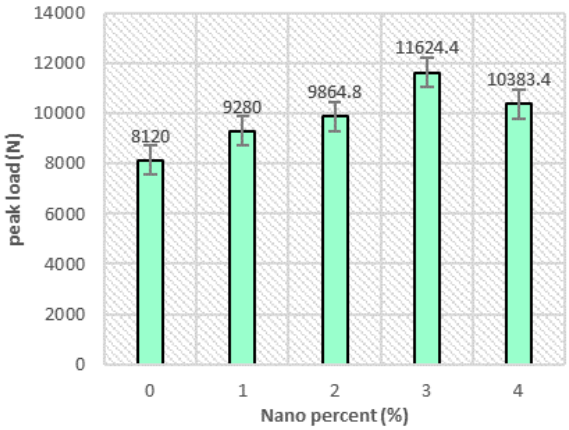

Fig. 17 Peak loads of fiber-reinforced specimens with different percentages of NS

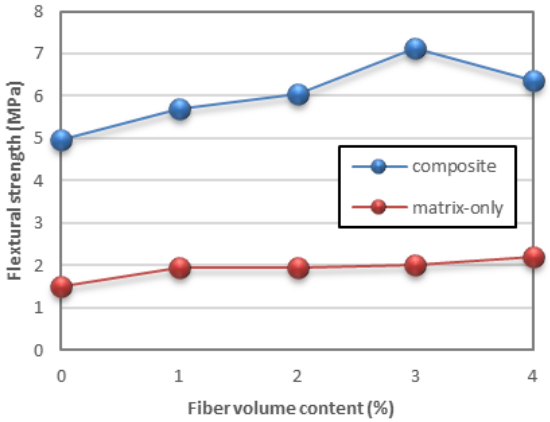

Fig. 18 Flexural strength of specimens with different percentages of NS

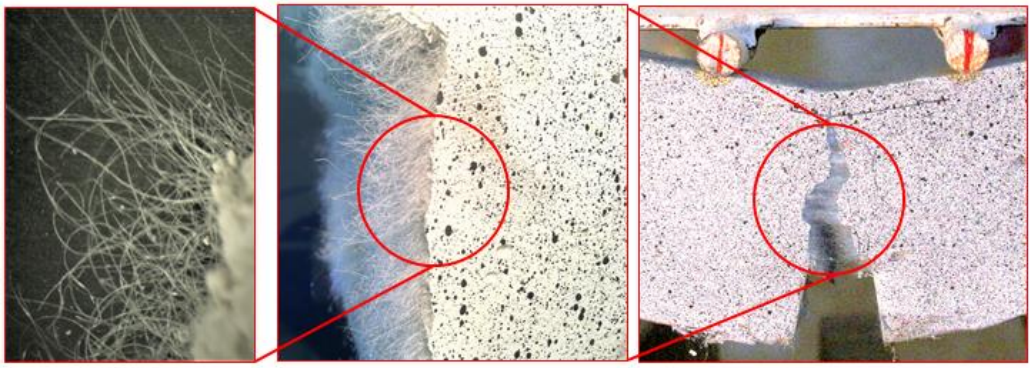

Fig. 19 Pullout of fibers from the matrix through the four-point bending test

reduces porosity. Nevertheless, the ideal amount of nano silica needed for achieving maximum flexural strength may differ depending on the specific application and requirements (Chaoshu *et al*. 2021).

4.4 Total fracture energy (GF), fiber pull out fracture energy (G_C), and matrix fracture toughness (J_{tip})

The total fracture energy and fiber pull-out fracture energy obtained from Eqs. 12 and 16 are given in Table 7. As shown in Fig. 19, fiber pull-out and fiber rupture occur after the peak load. As presented in Fig. 20, the fracture energy of fiber-reinforced cementitious composites increased with increasing NS up to 3%. However, with the increase of NS by 4%, the fracture energy reduced by 40%, in comparison with NS-3. The same trend happened for the pull-out fracture energy. Fig. 21 illustrates that adding NS in composites up to 4% reduced the G_C by 10% in comparison with NS-3. The results suggests that the fracture energy and fiber pull-out fracture energy of fiber-reinforced cementitious composites are significantly influenced by the addition of NS, which can be attributed to the nucleation effect and pozzolanic effect that enhance the interaction between the fiber and matrix, resulting in higher fracture energy and pull-out fracture energy.

Table 8 demonstrates the matrix fracture toughness corresponding to the NS percent, The matrix fracture toughness improved as the amount of NS increased. As

Table 6 Flexural strength with different NS percentages

Mix ID	flexural strength (MPa)	Mix ID	flexural strength (MPa)
NS-0, V-2	4.97	NS-0, V-0	1.5
NS-1, V-2	5.68	NS-1, V-0	1.9
NS-2, V-2	6.04	NS-2, V-0	1.95
NS-3, V-2	7.12	NS-3, V-0	2
NS-4, V-2	6.36	NS-4, V-0	2.2

Table 7 Fracture parameters, obtained from the load-deflection curve

Mix ID	G_F(N/mm)	G_C(N/mm)
NS-0	9.5	5.7
NS-1	11.9	6.5
NS-2	14	9.4
NS-3	16.6	10.6
NS-4	14.5	9.5

Table 8 Matrix fracture toughness of mixes with varying nano-silica content

Mix ID	J_{tip}(N/m)
NS-0	12.5
NS-1	14.7
NS-2	14.9
NS-3	15.9
NS-4	18.2

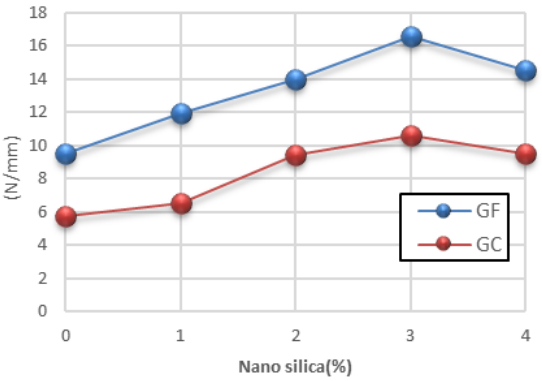

Fig. 20 Effect of NS percentages on the fracture energy and pull-out fracture energy of fiber-reinforced cementitious composites.

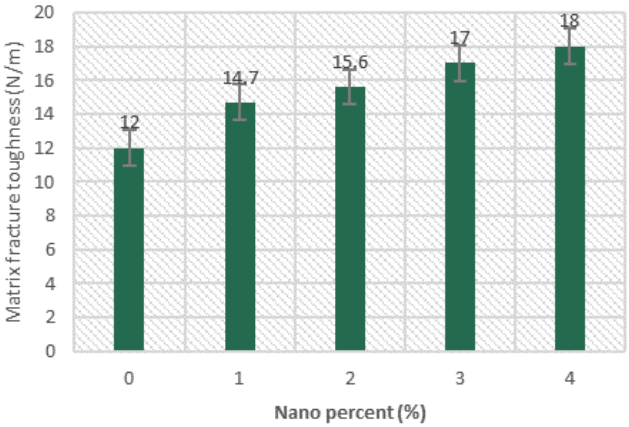

Fig. 21 Fracture toughness of cement-based matrix with different percentages of NS

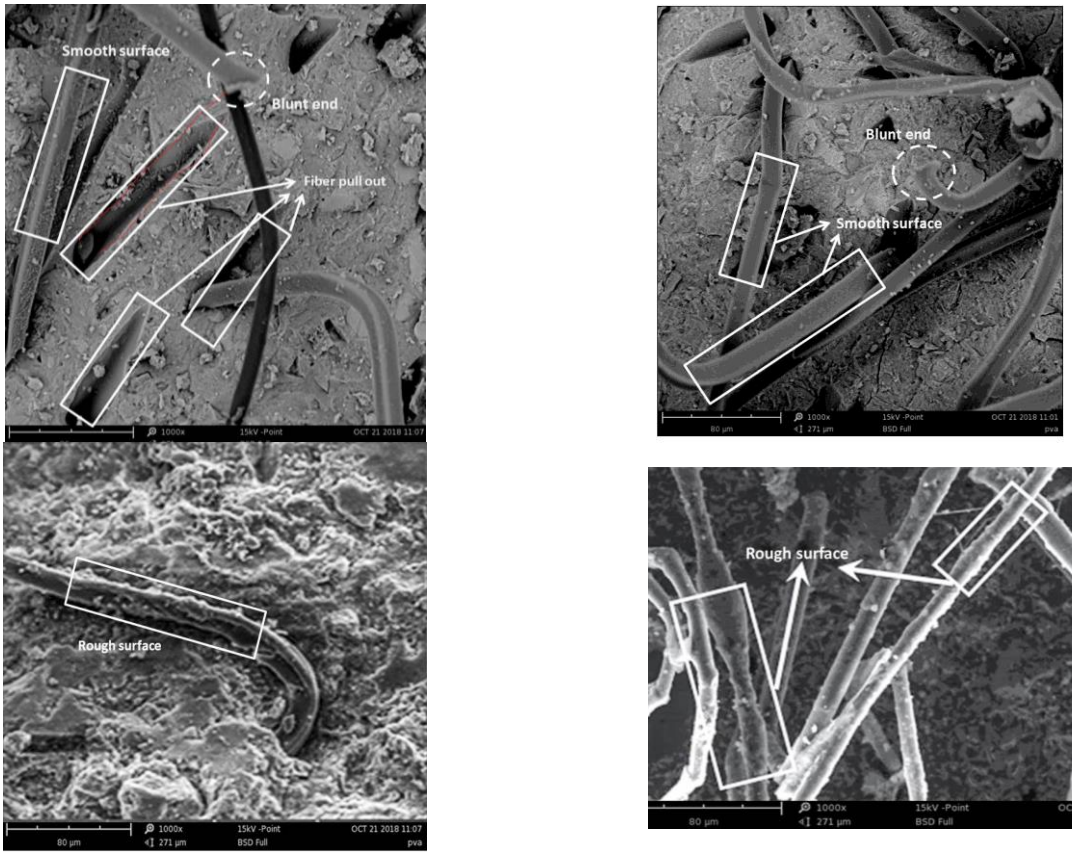

Fig. 22 Surfaces of the fibers in the composites: (a). Without NS (b). with 3% NS

Table 9 Micromechanics parameters

	Fiber parameters				Interface parameters			Matrix parameters	
Mix ID	$d_f(\mu m)$	$L_f(mm)$	$E_f(GPa)$	$\sigma_{fu}(Mpa)$	$G_d(^N/_{mm})$	f	G	$E_m(GPa)$	$J_{tip}(^N/_m)$
NS-0,V-2	35	18	3.5	400	0	0.7	1.78	2.50	12
NS-1,V-2	35	18	3.5	400	0	0.7	1.78	2.85	14.7
NS-2,V-2	35	18	3.5	400	0	0.7	1.78	2.86	15.6
NS-3,V-2	35	18	3.5	400	0	0.7	1.78	2.95	17
NS-4,V-2	35	18	3.5	400	0	0.7	1.78	3.15	18

Table 10 Frictional bond strength corresponds to total fracture energy and pull-out fracture energy

Mix ID	$G_c(^N/_{mm})$	$G_r(^N/_{mm})$	$\tau(MPa)$
NS-0,V-2	5.7	0.2	0.2
NS-1,V-2	6.5	0.28	0.24
NS-2,V-2	9.4	0.59	0.34
NS-3,V-2	10.6	0.75	0.39
NS-4,V-2	9.5	0.6	0.35

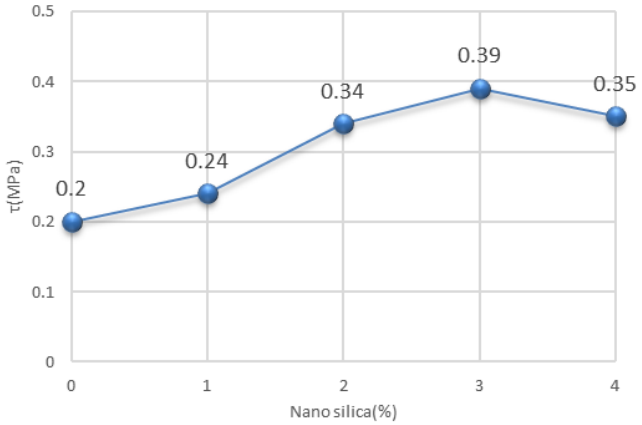

Fig. 23 Effect of different NS percentages on the Interfacial friction bond strength of fiber-reinforced cementitious composites

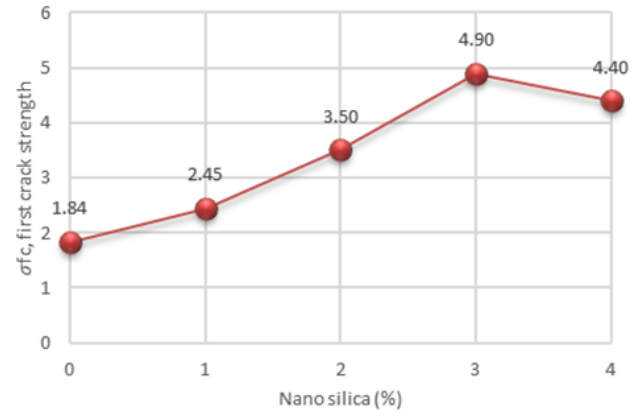

Fig. 24 Effect of different NS percentages on the first crack strength of the fiber-reinforced cementitious composite

mentioned before, it might be attributed to a better dispersion of NS particles in the matrix-only mixtures compared to FRCCs.

4.5 Interfacial friction bond strength (τ)

The micromechanical parameters related to the fibers, matrix, and interface of fiber/matrix are given in Table 9. The amount of chemical bonds in PP fibers is equal to zero. The value of the snubbing coefficient f is considered to be equal to 0.7, according to Li (Wang and Li 2007).

Interfacial friction bond strength (τ) is calculated by equating the G_C obtained from the area enclosed by the part of the load-displacement curve in which fiber pullout occurs and the Eq. 14. The values of τ, G_C and G_r are given in Table 10. As can be seen, the value of G_r is negligible compared to the value of G_C. Fig. 22 demonstrates the SEM photographs of the fracture surfaces of notched beam specimens, including composites with zero and 3% NS. Looking at Fig. 22, it is apparent that fibers in the specimen without any NS had no severe delamination failure during the pull-out process, and the fibers had intact and smooth surfaces, which is attributed to little chemical bonding and interfacial friction bond strength between matrix and fibers. In contrast, fibers in the specimens modified with 3% NS had rough surfaces attributed to the higher frictional bond strength leading to fiber rupture prevails over fiber pull out during the loading.

According to Fig. 23, it can be seen that increasing the NS up to 3% increased the interfacial friction bond strength. The addition of nano-silica (NS) can increase the interfacial bond strength by generating a more compact packing of hydration products, refining the matrix's pore structure, and enhancing the interfacial transition zone (ITZ) between the hardened paste and fibers. It is also worth noting that, as stated in the previous sections, higher interfacial friction bond strength between fibers and matrix resulted in higher tensile and flexural strengths. Adding NS more than 3% strengthens the matrix, and rupture mode prevails over the sliding mode of failure in fibers, which results in reducing the interfacial friction bond strength.

4.6 First cracking strength

By monitoring the formation and growth of cracks during the test, it was discovered that increasing the percentage of NS in the mixtures increased the specimen's first cracking strength (Fig. 24). Fig. 25 shows an overview of the initiation and propagation of the crack utilizing digital image correlation (DIC). It can be seen from Fig. 25, multiple cracks occurred during the loading, cracks are shown by red lines.

4.7 The maximum bridging stress (σ_{pc})

As shown in Fig. 26, the maximum bridging stress (σ_{pc}) obtained from Eq. 4 increased by increasing NS from 1 up to 3%. However, in the composite with NS of more than 3%, this trend will be decreasing. The bridging stress via opening displacement curves of the crack in mixes with different NS percent are shown in Fig. 27. The mixture with

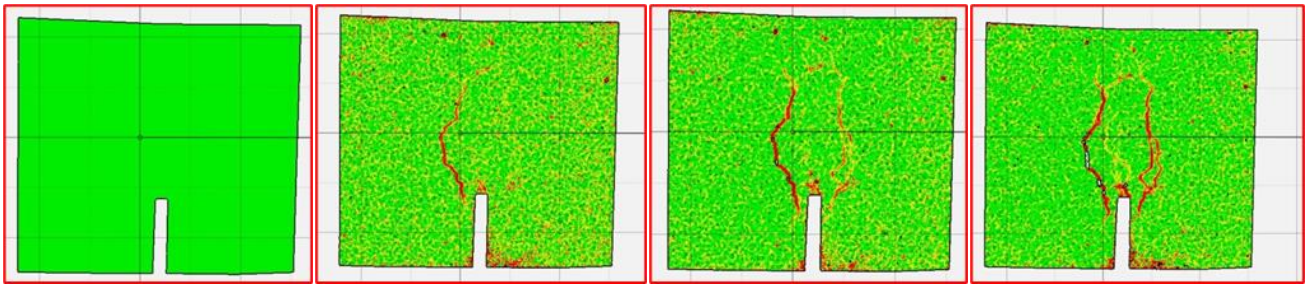

Fig. 25 Monitoring the initiation and propagation of the cracks during the loading utilizing DIC

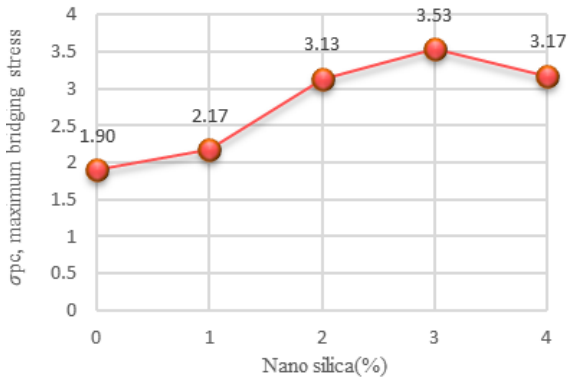

Fig. 26 Effect of NS on fiber-reinforced cementitious composites' maximum bridging stress

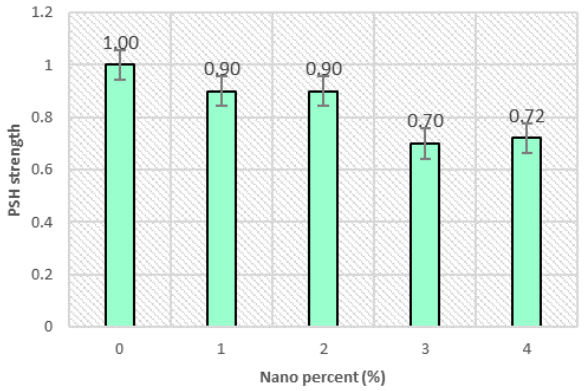

Fig. 28 PSH strength in cementitious composite with different percentages of NS

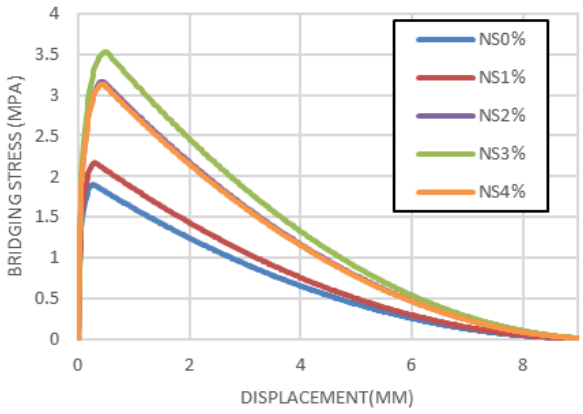

Fig. 27 bridging stress via opening displacement in mixes with different percentages of NS

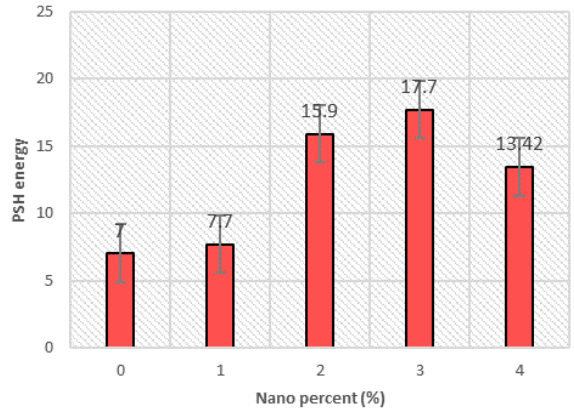

Fig. 29 PSH energy in cementitious composite with different percentages of NS

3% NS has a better performance in comparison with the rest of the mixes.

4.8 Pseudo-strain-hardening (PSH) indices

As aforementioned, two PSH performance indexes are used to evaluate the hardening behavior of cementitious composites quantitatively. The higher the margin, the closer the composite behavior is to the hardening behavior.

As demonstrated in Fig. 28, with the increasing of NS percent and therefore increasing the toughness of the cement matrix, the PSH strength index reduced. This can be attributed to the fact that a strong matrix prevents multiple cracking. So, strengthening the matrix reduces the hardening behavior of FRCCs.

In contrast to the PSH strength index, increasing NS content up to 3% leads to an increase in the PSH energy index which might be attributed to the enhancement in the frictional bond strength of the fibers. This finding is consistent with the results of a study conducted by Chaoshu *et al*. (2021), which demonstrated that the addition of NS enhanced both the fracture toughness of the matrix and the fiber bridging performance of lightweight engineered cementitious composites. What stands out from Figs. 28 and 29 is that the PSH energy index was more sensitive to changes in the percentage of NS.

(a)

(b)

Fig. 30 Multiple cracking of specimen under four point bending test, (a) NS = 0% (b) NS = 3%

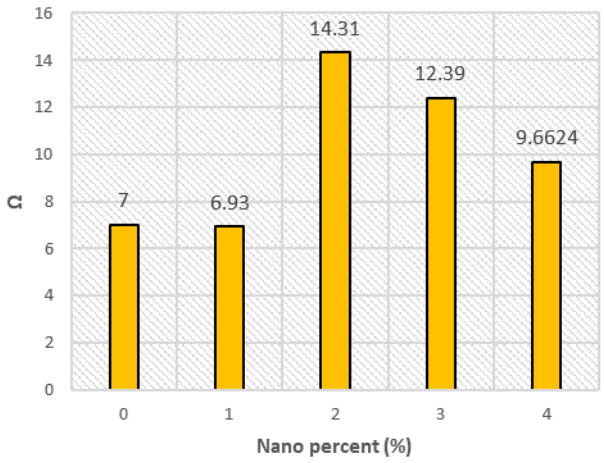

Fig. 31 Ω index values in cementitious composite with different percentages of NS

As it can be seen from Fig. 30, increasing the NS content led to an increase in the maximum crack width of the specimen from 40 μm in the NS0 up to 110 μm in the NS3. This confirmed the fact that there is a significant correlation between maximum crack width and higher strength of the matrix.

It is worthy to mention that the enhancement in the frictional strength strengthens the slip hardening in the composites leading to an increase in the rupture failure modes of the fibers and resistance against the pull out of the fibers. Limiting the frictional strength is necessary to achieve steady-state crack propagation and multiple cracking, which are characteristics of ductile composites. In order to achieve steady-state crack propagation in composites with a certain matrix toughness, an optimal range of frictional stress is required. If the frictional stress falls below the minimum value, it can facilitate the pull-out failure mode of fibers, whereas if it exceeds the maximum value, it can lead to fiber rupture. To produce a cementitious composite with both ductility and high tensile strength, it is crucial to strike a balance between the percentages of fibers exhibiting pull-out failure mode and rupture failure mode. To find the optimum value of NS percent and subsequently the optimum value of the frictional strength a new criterion (Ω) defined as:

$$\Omega = PSH_{strength}.PSH_{energy} \tag{18}$$

It can be seen from Fig. 31, the Ω value of the mixture with 2% NS is higher than that of the rest of the mixtures. Although it seems that the mixture with 3% NS has the best mechanical properties, the optimum percentage in which both ductility and high tensile strength of the composites would be satisfied is 2%.

5. Conclusions

In this research, to replace part of cement with supplementary cementitious materials, GGBFS was used to produce a composite with strain hardening behavior. For modifying the drawbacks of adding large amounts of pozzolanic materials, different percentages of NS were used. The micromechanics principles were utilized to guide the design process aimed at maximizing the strain-hardening potential. In this regard, a novel technique was proposed to investigate the micromechanical parameters from the fractural test, and micromechanical relations are adapted to use in the proposed method. Digital image correlation (DIC) was used for monitoring the onset and propagation of the cracks.

To find the optimum percent of NS a new criterion was supposed to balance between the percentage of fibers with pull-out failure mode and rupture failure mode to have a cementitious composite with ductility as well as high tensile strength. It became clear that micromechanical analysis should be used instead of trial and error in producing cementitious composites. From the obtained results of this research, the following main conclusions could be drawn:

• The results of this research support the idea that the addition of NS particles decreases the amount of lubrication water leading to a reduction in flow values.

• The 28-day compressive strength of fiber-reinforced composites was enhanced by adding 3% NS particles because of the filling effect along with the chemical effect of NS particles.

• All of the modified composites displayed deflection hardening behavior. Additionally, the flexural strength of

green cementitious composite increased with the addition of NS up to 3%.

• Increasing the NS content in the mixtures, resulted in strengthening the cementitious matrix and increasing the matrix fracture toughness. It was observed that increasing the NS percent has an enhancing effect on the flexural first crack strength. Moreover, by increasing NS up to 3%, fracture energy, rupture fracture energy, pull-out fracture energy, and maximum bridging stress of cementitious composite all increased. Then adding more NS had a negative effect on fracture and micromechanics parameters.

• Using the results of the three-point beam, It was found that over increasing NS percent, rupture failure of fibers prevails over fiber pull out. SEM analysis confirmed the fact that the fibers' surface with the addition of NS had a rough surface, in contrast to unmodified composites in which the surface of the fibers was smooth and intact.

• Adding NS up to 3% increased the PSH energy and decreased the PSH strength. It was also found that the PSH energy index was more sensitive to the content of NS percent.

• The results of this research highlighted the importance of finding the optimum NS percent to make a balance between the percentages of fibers with pull-out failure mode and rupture failure mode to have an engineered cementitious composite with ductility as well as high tensile strength. Consequently, a new criterion (Ω) was defined. Although it seems that the mixture with 3 percent NS has the best mechanical and fractural properties, the optimum percent in which both ductility and high tensile strength of the composites would be satisfied is 2%.

Acknowledgment

This work was supported by Shahid Rajaee Teacher Training University under grant number 4951.

References

Abna, A. and Mazloom, M. (2022), "Flexural properties of fiber reinforced concrete containing silica fume and nano-silica", *Mater. Lett.*, **316**, 132003. https://doi.org/10.1016/j.matlet.2022.132003

ASTM C1609 / C1609M-19a (2019), Standard Test Method for Flexural Performance of Fiber-Reinforced Concrete (Using Beam With Third-Point Loading), ASTM International, West Conshohocken, Pennsylvania, U.S.A. https://doi.org/10.1520/C1609_C1609M-19A.

Bhosale, A.B., Lakavath, C. and Prakash, S.S. (2020), "Multi-linear tensile stress-crack width relationships for hybrid fibre reinforced concrete using inverse analysis and digital image correlation", *Eng. Struct.*, **225**, 111275. https://doi.org/10.1016/j.engstruct.2020.111275

Björnström, J., Martinelli, A., Matic, A., Börjesson, L. and Panas, I. (2004), "Accelerating effects of colloidal nano-silica for beneficial calcium–silicate–hydrate formation in cement", *Chem. Phys. Lett.*, **392**(1-3), 242-248. https://doi.org/10.1016/j.cplett.2004.05.071.

Reddy, K.C. and Subramaniam, K.V. (2017), "Analysis for multi-linear stress-crack opening cohesive relationship: application to macro-synthetic fiber reinforced concrete", *Eng. Fract. Mech.*, **169**, 128-45. https://doi.org/10.1016/j.engfracmech.2016.11.015.

C. Li V. (1992), "Postcrack scaling relations for fiber reinforced cementitious composites", *J. Mater. Civil Eng.*, **4**(1), 41-57. https://doi.org/10.1061/(ASCE)0899-1561(1992)4:1(41).

Diamantonis, N., Marinos, I., Katsiotis, M. S., Sakellariou, A., Papathanasiou, A., Kaloidas, V. and Katsioti, M. (2010), "Investigations about the influence of fine additives on the viscosity of cement paste for self-compacting concrete", *Constr Build Mater*. **24**(8), 1518-1522. https://doi.org/10.1016/j.conbuildmat.2010.02.005.

Flores-Vivian I, Pradoto R, Moini M, Sobolev K. 2013. "The use of nanoparticles to improve the performance of concrete", *5th Inter. Nano Conference*. Czech Republic, EU, ocotber.

Flores-Vivian, I., Pradoto, R., Moini, M. and Sobolev, K. (2013), "The use of nanoparticles to improve the performance of concrete", *Proceedings of the 5th International Nano Conference*, Czech Republic, EU, ocotber.

Fu, C., Guo, R., Lin, Z., Xia, H., Yang, Y. and Ma, Q. (2021), "Effect of nanosilica and silica fume on the mechanical properties and microstructure of lightweight engineered cementitious composites", *Constr. Build. Mater.*, **298**, 123788. https://doi.org/10.1016/j.conbuildmat.2021.123788

Goh SW, You Z. (2009), "A simple stepwise method to determine and evaluate the initiation of tertiary flow for asphalt mixtures under dynamic creep test", *Constr Build Mater*. **23**(11):3398-3405. https://doi.org/10.1016/j.conbuildmat.2009.06.020.

Hanehara, S., Tomosawa, F., Kobayakawa, M. and Hwang, K. (2001), "Effects of water/powder ratio, mixing ratio of fly ash, and curing temperature on pozzolanic reaction of fly ash in cement paste", *Cem. Concr. Res.*, **31**(1), 31-39. https://doi.org/10.1016/S0008-846(00)00441-5.

Hejazi, S.M., Sheikhzadeh, M., Abtahi, S.M. and Zadhoush, A. (2012), "A simple review of soil reinforcement by using natural and synthetic fibers", *Constr. Build. Mater.*, **30**, 100-116. https://doi.org/10.1016/j.conbuildmat.2011.11.045.

Hillerborg, A. (1980), "Analysis of fracture by means of the fictitious crack model, particularly for fibre reinforced concrete", *Int. J. Cement Compos.*, **2**(4), 177-184.

Hillerborg, A. (1985), "The theoretical basis of a method to determine the fracture energyGF of concrete", *Mater Struct.* **18**(4), 291-296. https://doi.org/10.1007/BF02472919.

Hillerborg, A., Modéer, M. and Petersson, P.E. (1976), "Analysis of crack formation and crack growth in concrete by means of fracture mechanics and finite elements", *Cem. Concr. Res.*, **6**(6), 773-781. https://doi.org/10.1016/0008-8846(76)90007-7.

Ji, T. (2005), "Preliminary study on the water permeability and microstructure of concrete incorporating nano-SiO2", *Cem Concr Res***. 35**(10), 1943-1947. https://doi.org/10.1016/j.cemconres.2005.07.004.

Jo, B.W., Kim, C.H., Tae, G.H. and Park, J.B. (2007), "Characteristics of cement mortar with nano-SiO2 particles", *Constr Build Mater*. **21**(6), 1351-1355. https://doi.org/10.1016/j.conbuildmat.2005.12.020.

Karamloo, M. and Mazloom, M. (2018), "An efficient algorithm for scaling problem of notched beam specimens with various notch-to-depth ratios", *Comput. Concr*, **22**(1), 39-51. http://doi.org/10.12989/cac.2018.22.1.039.

Karimpour, H. and Mazloom, M. (2022a), "Pseudo-strain hardening and mechanical properties of green cementitious composites containing polypropylene fibers", *Struct. Eng. Mech.*, **81**(5), 575. https://doi.org/10.12989/sem.2022.81.5.575

Karimpour, H. and Mazloom, M. (2022b), "Determining a novel softening function for modeling the fracture of concrete", *Adv. Mater. Res.*, **11**(4), 351-374. https://doi.org/10.12989/amr.2022.11.4.351

Kawashima, S., Hou, P., Corr, D.J. and Shah, S.P. (2013), "Modification of cement-based materials with nanoparticles", *Cem. Concr. Compos.*, **36**, 8-15. https://doi.org/10.1016/00225096(91)90043-N.

Kim, J.K., Kim, J.S., Ha, G.J. and Kim, Y.Y. (2007), "Tensile and fiber dispersion performance of ECC (engineered cementitious composites) produced with ground granulated blast furnace slag", *Cem. Concr. Res.*, **37**(7), 1096-1105. https://doi.org/10.1016/j.cemconres.2007.04.006.

Lepech, M.D., Li, V.C., Robertson, R.E. and Keoleian, G.A. (2008), "Design of green engineered cementitious composites for improved sustainability", *ACI Mater. J.*, **105**(6), 567.

Li, G. (2004), "Properties of high-volume fly ash concrete incorporating nano-SiO2", *Cem. Concr. Res.*, **34**(6), 1043-1049. https://doi.org/10.1016/j.cemconres.2003.11.013.

Li, Q., Gao, X., Xu, S. (2016), "Multiple effects of nano-SiO2 and hybrid fibers on properties of high toughness fiber reinforced cementitious composites with high-volume fly ash", *Cem. Concr. Compos.*, **72**, 201-212. https://doi.org/10.1016/j.cemconcomp.2016.05.011.

Li, V.C. (1993), "From micromechanics to structural engineering-the design of cementitous composites for civil engineering applications", *J. Struct. Mech, Earthq. Eng.*, **471**, 1-12. https://doi.org/10.2208/jscej.1993.471_1.

Li, V.C. (2002), "Advances in ECC research", *ACI Spec Publ.*, **206**, 373-400.

Li, V.C. (2003a), "On engineered cementitious composites (ECC)", *J. Adv. Concr. Technol.*, **1**(3), 215-230. https://doi.org/10.3151/jact.1.215.

Li, V.C. (2003b), "On engineered cementitious composites (ECC) a review of the material and its applications", *J. Adv. Concr. Technol.*, **1**(3), 215-230. https://doi.org/10.3151/jact.1.215.

Li, V.C. (2019), *Engineered Cementitious Composites (ECC), Bendable Concrete for Sustainable and Resilient Infrastructure*, Springer, Springer-Verlag, Berlin, Heidelberg.

Li, V.C., Wang, Y., Backer, S. (1991), "A micromechanical model of tension-softening and bridging toughening of short random fiber reinforced brittle matrix composites", *J. Mech. Phys. Solids*, **39**(5), 607-625. https://doi.org/10.1016/0022-5096(91)90043-N.

Lin, Z., Li, V.C. (1997), "Crack bridging in fiber reinforced cementitious composites with slip-hardening interfaces", *J. Mech. Phys. Solids*, **45**(5), 763-787. https://doi.org/10.1016/S0022-5096(96)00095-6.

Marshall, D.B., Cox, B.N. (1988), "A J-integral method for calculating steady-state matrix cracking stresses in composites", *Mech. Mater.*, **7**(2), 127-133. https://doi.org/10.1016/0167-6636(88)90011-7.

Mazloom, M. and Mirzamohammadi, S. (2019), "Thermal effects on the mechanical properties of cement mortars reinforced with aramid, glass, basalt, and polypropylene fibers", *Adv. Mater. Res.*, **8**(2), 137-154. http://doi.org/10.12989/amr.2019.8.2.137.

Mazloom, M. and Mirzamohammadi, S. (2021), "Fracture of fiber-reinforced cementitious composites after exposure to elevated temperatures", *Mag. Concr. Res.*, **73**(14), 701-713. https://doi.org/10.1680/jmacr.19.00401.

Mazloom, M. and Salehi, H. (2018), "The relationship between fracture toughness and compressive strength of self-compacting lightweight concrete", *IOP Conference Series: Mater. Sci. Eng.*, **431**(6). https://doi.org/10.1088/1757-899X/431/6/062007.

Mazloom, M., Karimpanah, H. and Karamloo, M. (2020), "Fracture behavior of monotype and hybrid fiber reinforced self-compacting concrete at different temperatures", *Adv. Concr. Constr.*, **9**(4), 375-386. https://doi.org/10.12989/acc.2020.9.4.375.

Mazloom, M., Soltani, A., Karamloo, M., Hassanloo, A. and Ranjbar, A. (2018), "Effects of silica fume, superplasticizer dosage and type of superplasticizer on the properties of normal and self-compacting concrete", *Adv Mater Res.* **7**(1), 45. http://doi.org/10.12989/amr.2018.7.1.045.

Mitrović, A., Antonović, D., Tanasić, I., Mitrović, N., Bakić, G., Popović, D. and Milošević, M. (2019), "3D digital image correlation analysis of the shrinkage strain in four dual cure composite cements", *BioMed Res. Int.*, 2041348. https://doi.org/10.1155/2019/2041348.

Mehta, P. and Monteiro, P. (2017), *Concrete Microstructure, Properties and Materials*, McGraw-Hill Education.

Mohammed, B.S., Achara, B.E., Nuruddin, M.F., Yaw, M. and Zulkefli, M.Z. (2017), "Properties of nano-silica-modified self-compacting engineered cementitious composites", *J. Clean Prod.*, **162**, 1225-1238. https://doi.org/10.1016/j.jclepro.2017.06.137.

Naaman, A.E. and Najm, H. (1991), "Bond-slip mechanisms of steel fibers in concrete", *ACI Mater. J.*, **88**(1991), 135-145.

Naniz, O.A., Mazloom, M. (2018), "Effects of colloidal nano-silica on fresh and hardened properties of self-compacting lightweight concrete", *J. Build. Eng.*, **20**, 400-410. https://doi.org/10.1016/j.jobe.2018.08.014.

Neville, A.M. (1996), *Properties of Concrete*, ELBS with Addison Wesley Longman Limited.

Newman, J. and Choo, B.S. (2003), "Advanced concrete technology", *Adv. Concr. Technol.*, 1-1433. https://doi.org/10.1016/B978-0-7506-5686-3.X5246-X.

Pan, Z., Wu, C., Liu, J., Wang. W. and Liu, J. (2015), "Study on mechanical properties of cost-effective polyvinyl alcohol engineered cementitious composites (PVA-ECC)", *Constr. Build Mater.*, **78**, 397-404. https://doi.org/10.1016/j.conbuildmat.2014.12.071.

Petersson, P.E. (1981), "Crack growth and development of fracture zones in plain concrete and similar materials", Doctoral dissertation, Lund University, Sweden.

Poon, C.S., Lam, L. and Wong, Y.L. (2000), "A study on high strength concrete prepared with large volumes of low calcium fly ash", *Cem. Concr. Res.*, **30**(3), 447-455. https://doi.org/10.1016/S0008-8846(99)00271-9.

Poppe, A.M. and De Schutter, G. (2005), "Cement hydration in the presence of high filler contents", *Cem. Concr. Res.*, **35**(12), 2290-2299. https://doi.org/10.1016/j.cemconres.2005.03.008.

Pourjavadi, A., Fakoorpoor, S.M., Khaloo, A. and Hosseini, P. (2012), "Improving the performance of cement-based composites containing superabsorbent polymers by utilization of nano-SiO2 particles", *Mater. Des.*, **42**, 94-101. https://doi.org/10.1016/j.matdes.2012.05.030.

Qian, S. and Li, V.C. (2008), "Simplified inverse method for determining the tensile properties of strain hardening cementitious composites (SHCC)", *J. Adv. Concr. Technol.*, **6**(2), 353-363.https://doi.org/10.3151/jact.6.353

Qing, Y., Zenan, Z., Deyu, K. and Rongshen, C. (2007), "Influence of nano-SiO2 addition on properties of hardened cement paste as compared with silica fume", *Constr. Build Mater.*, **21**(3), 539-545. https://doi.org/10.1016/j.conbuildmat.2005.09.001.

Rice, J.R. (1968), "A path independent integral and the approximate analysis of strain concentration by notches and cracks", *J. Appl. Mech.* **35**(2), 379-386. https://doi.org/10.1115/1.3601206.

Rilem, D.R. (1985), "Determination of the fracture energy of mortar and concrete by means of three-point bend tests on notched beams", *Mater. Struct.*, **18**(106), 285-290.

Rooke, D.P. and Cartwright, D.J. (1976), *Compendium of Stress Intensity Factors*, Procure Exec Minist Defence HMSO.

Salehi, H. and Mazloom, M. (2018), "Effect of magnetic-field intensity on fracture behaviors of self-compacting lightweight concrete", *Mag. Concr. Res.*, **71**(13), 665-679.

https://doi.org/10.1680/jmacr.17.00418.
Senff, L., Labrincha, J.A., Ferreira, V.M., Hotza, D. and Repette, W.L. (2009), "Effect of nano-silica on rheology and fresh properties of cement pastes and mortars", *Constr. Build. Mater.*, **23**(7), 2487-2491. https://doi.org/10.1016/j.conbuildmat.2009.02.005.
Shah, S.P., Konsta-Gdoutos, M.S., Metaxa, Z.S., Mondal, P. (2009), *Nanoscale Modification of Cementitious Materials*, In *Nanotechnology in Construction*, Springer. https://doi.org/10.1007/978-3-642-00980-8_16.
Swaddiwudhipong, S., Lu, H.R., Wee, T.H. (2003), "Direct tension test and tensile strain capacity of concrete at early age", *Cem. Concr. Res.*, **33**(12), 2077-2084. https://doi.org/10.1016/S0008-8846(03)00231-X.
Torabian Isfahani, F., Redaelli, E., Li, W. and Sun, Y. (2017), "Effects of nanosilica on early age stages of cement hydration", *J. Nanomater.*, 4687484. https://doi.org/10.1155/2017/4687484.
Tsivilis, S., Batis, G., Chaniotakis, E., Grigoriadis, G. and Theodossis, D. (2000), "Properties and behavior of limestone cement concrete and mortar", *Cem. Concr. Res.*, **30**(10), 1679-1683. http://doi.org/10.1016/S0008-8846(00)00372-0.
Wang, S. and Li, V.C. (2007), "Engineered cementitious composites with high-volume fly ash", *ACI Mater. J.*, **104**(3), 233.
Yang, E.H., Li, V.C. (2010), "Strain-hardening fiber cement optimization and component tailoring by means of a micromechanical model", *Constr. Build Mater.*, **24**(2), 130-139. https://doi.org/10.1016/j.conbuildmat.2007.05.014.
Yon, J.H., Hawkins, N.M., Kobayashi, A.S. (1997), "Comparisons of concrete fracture models", *J. Eng. Mech.*, **123**(3), 196-203. https://doi.org/10.1061/(ASCE)0733-9399(1997)123:3(196).
Zhang, J. and Li, V.C. (2002), "Effect of inclination angle on fiber rupture load in fiber reinforced cementitious composites", *Compos. Sci. Technol.*, **62**(6), 775-781. https://doi.org/10.1016/S0266-3538(02)00045-3
Zhang, Y.M., Sun, W. and Yan, H.D. (2000), "Hydration of high-volume fly ash cement pastes", *Cem. Concr. Compos.*, **22**(6), 445-452. https://doi.org/10.1016/S0958-9465(00)00044-5.
Zhou, J., Qian, S., Beltran, M.G.S., Ye, G., van Breugel, K., Li, V.C. (2010), "Development of engineered cementitious composites with limestone powder and blast furnace slag", *Mater. Struct.*, **43**(6), 803-814. http://doi.org/10.1617/s11527-009-9549-0.
Zhou, J., Qian, S., Ye, G., Copuroglu, O., van Breugel, K., Li, V.C. (2012), "Improved fiber distribution and mechanical properties of engineered cementitious composites by adjusting the mixing sequence", *Cem. Concr. Compos.*, **34**(3), 342-348. https://doi.org/10.1016/j.cemconcomp.2011.11.019.

CC